Graphene Networks Anchored with Sn@Graphene as Lithium Ion Battery Anode
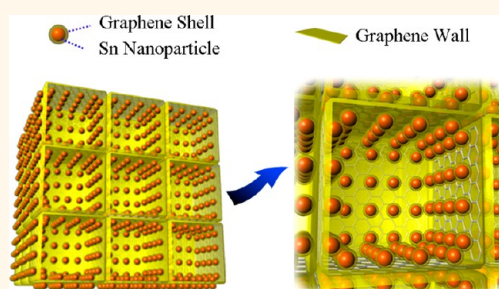
Jian Qin,[†] Chunnian He,[†,‡,*] Naiqin Zhao,[†,‡,*] Zhiyuan Wang,[†] Chunsheng Shi,[†] En-Zuo Liu,[†] and Jiajun Li[†]

[†]School of Materials Science and Engineering and Tianjin Key Laboratory of Composites and Functional Materials, Tianjin University, Tianjin 300072, China, and [‡]Collaborative Innovation Center of Chemical Science and Engineering, Tianjin 300072, China

ABSTRACT A facile and scalable *in situ* chemical vapor deposition (CVD) technique using metal precursors as a catalyst and a three-dimensional (3D) self-assembly of NaCl particles as a template is developed for one-step fabrication of 3D porous graphene networks anchored with Sn nanoparticles (5–30 nm) encapsulated with graphene shells of about 1 nm (Sn@G-PGNWs) as a superior lithium ion battery anode. In the constructed architecture, the CVD-synthesized graphene shells with excellent elasticity can effectively not only avoid the direct exposure of encapsulated Sn to the electrolyte and preserve the structural and interfacial stabilization of Sn nanoparticles but also suppress the aggregation of Sn nanoparticles and buffer the volume expansion, while the interconnected 3D porous graphene networks with high electrical conductivity, large surface area, and high mechanical flexibility tightly pin the core–shell structure of Sn@G and thus lead to remarkably enhanced electrical conductivity and structural integrity of the overall electrode. As a consequence, this 3D hybrid anode exhibits very high rate performance (1022 mAh/g at 0.2 C, 865 mAh/g at 0.5 C, 780 mAh/g at 1 C, 652 mAh/g at 2 C, 459 mAh/g at 5 C, and 270 mAh/g at 10 C, 1 C = 1 A/g) and extremely long cycling stability even at high rates (a high capacity of 682 mAh/g is achieved at 2 A/g and is maintained approximately 96.3% after 1000 cycles). As far as we know, this is the best rate capacity and longest cycle life ever reported for a Sn-based lithium ion battery anode.

KEYWORDS: Sn · graphene · high-rate · core–shell · nanohybrid · 3D network · *in situ* synthesis · chemical vapor deposition · lithium storage

The requirement in developing lithium ion batteries (LIBs) with high power and energy density has been increasing to satisfy the urgent needs for application in electric vehicles and power grids.[1] However, current commercial graphite anodes with a low theoretical capacity of 372 mAh/g give rise to a very limited energy output for LIBs, and alternative anode materials with higher reversible and rate capacities as well as long-term cyclic stability are highly desired.[1] In this context, metallic Sn, which not only has high theoretical capacity (993 mAh/g or 7262 mAh/cm^3 for Li$_{4.4}$Sn) and electronic conductivity but also has moderate operating voltage that can improve the safety of LIBs during the rapid charge/discharge process,[2–4] has been extensively explored as a promising alternative anode material for high-performance LIBs. Unfortunately, a dramatic volume change (about 300%) commonly

occurs in Sn during lithium ion insertion/extraction, which causes not only severe pulverization and subsequent electrical disconnection from the current collector but also aggregation of Sn nanoparticles and continual formation of a very thick solid electrolyte interphase (SEI) on the Sn surfaces upon cycling, thereby leading to rapid capacity decay and poor cyclability.[2–4] To overcome these issues, substantial efforts have been made to improve the structural stability and integrity of Sn anodes, such as synthesizing Sn nanostructures[4,5] and constructing hybrid anodes consisting of nanosized Sn and carbon. A wide variety of Sn–carbon hybrids such as Sn nanoparticles embedded in porous carbon,[6–15] Sn or Sn@C nanoparticles encapsulated with carbon nanotubes,[16–20] and carbon-encapsulated Sn nanostructures[21–24] have been designed. These carbon matrices can provide spaces to buffer the mechanical

stress induced by the volume change of the Sn nanostructures, resulting in significantly improved cycling performance. However, up to now long cycle life over hundreds of cycles at high rates still has not been achieved for these Sn—carbon hybrid anodes.

Recently, a novel two-dimensional graphitic carbon, graphene, has drawn special attention and is preferable to replace other types of carbon materials (*e.g.*, graphite, porous carbon, carbon nanotubes) to support metal or metal oxides for further enhancing of the electrochemical performances of LIB electrodes due to its outstanding electrical conductivity, superior mechanical flexibility, large specific surface area, and high thermal/chemical stability.[25,26] Hence, many Sn—graphene hybrids with various structures such as directly decorated Sn—graphene,[27−31] Sn@C-graphene,[32,33] and sandwich-like graphene-supported hybrids[34−38] have been developed. Although improved electrochemical performances have been achieved in these hybrid anodes, their rate performances and cycling stability at high charge/discharge rates are not superior to or even worse than that of the other Sn—carbon hybrid anodes. This may be attributed to the following factors: (i) the graphene nanosheets are very prone to irreversible aggregation or restacking due to the strong van der Waals forces among individual graphene nanosheets, resulting in a seriously reduced active surface area and porous structure compared with anticipated data;[39] (ii) the graphene materials employed in these hybrids are derived from reduced graphene oxide (rGO), which has severe structural defects introduced during exfoliation and reduction processes, leading to poor electron conductivity and structural stability. In the case of high charge/discharge rates during cycling, their stability and performances are rather low;[39] (iii) the size and dispersion uniformity of Sn nanoparticles in the graphene have not been efficiently controlled due to their low melting point (only 232 °C), which would accelerate the coalescence of Sn into large particles during the high temperature synthesis processes required in most cases;[6,35] (iv) in some Sn—graphene hybrids,[20−22] the exposed active Sn nanostructures, which are simply decorated on the surface of graphene nanosheets, would directly contact the electrolyte and thus result in side reactions at the interface between Sn and the electrolyte; meanwhile, the volume expansion and aggregation of these active nanostructures are hard to avoid during the cycle processes due to the nonintimate contact between graphene nanosheets and active materials.[40] Therefore, it is very urgent to develop Sn—graphene hybrids with unique structures that can circumvent the aggregation of Sn nanostructures and graphene nanosheets as well as keep the overall electrode highly conductive, active, and integrated during the high-rate charge/discharge process.[40]

Herein, we report a novel and scalable *in situ* chemical vapor deposition (CVD) technique using metal precursors as a catalyst and a three-dimensional (3D) self-assembly of NaCl particles as a template for one-step fabrication of 3D porous graphene networks anchored with Sn nanoparticles encapsulated with graphene shells (designated as Sn@G-PGNWs) as a superior LIB anode. This novel strategy for preparing 3D Sn@G-PGNWs with great conductivity and large surface area involves self-assembly of water-soluble NaCl particles uniformly coated with an ultrathin film of $SnCl_2$—$C_6H_8O_7$ into a 3D structure by freeze-drying technology and subsequent calcination of this 3D $SnCl_2$—$C_6H_8O_7$/NaCl in a hydrogen environment to reduce the metal precursors into small and homogeneous Sn nanoparticles, which can function as a catalyst for the subsequent growth of graphene walls between NaCl surfaces and graphene shells on the Sn surface. This process produces 3D Sn@G-PGNW hybrids in which the *in situ* synthesized Sn nanoparticles (5−30 nm) encapsulated with conformal and thin graphene shells (∼1 nm) are very homogeneously and tightly pinned on the surfaces of thin walls (≤3 nm) of 3D porous graphene networks. In this constructed unique 3D hybrid architecture, the CVD-synthesized graphene shells with excellent elasticity can effectively not only avoid the direct exposure of encapsulated Sn to the electrolyte and preserve the structural and interfacial stabilization of Sn nanoparticles but also suppress the aggregation of Sn nanoparticles and buffer the volume expansion,[41,42] while the interconnected 3D porous graphene networks with high electrical conductivity, large surface area, and high mechanical flexibility[43−46] tightly pin the core—shell structure of Sn@G and thus lead to remarkably enhanced electrical conductivity and structural integrity of the overall electrode.[47] As a consequence, this novel hybrid anode exhibits very high rate performance (1022 mAh/g at 0.2 C, 865 mAh/g at 0.5 C, 780 mAh/g at 1 C, 652 mAh/g at 2 C, 459 mAh/g at 5 C, and 270 mAh/g at 10 C, 1 C = 1 A/g) and extremely long cycling stability even at high rates (a high capacity of 682 mAh/g is achieved at 2 A/g and is maintained approximately 96.3% after 1000 cycles). As far as we know, this is the best rate capacity and longest cycle life ever reported for a Sn-based lithium ion battery anode.

RESULTS AND DISCUSSION

The overall synthetic procedure leading to 3D Sn@G-PGNWs is illustrated in Figure 1. During the synthesis, two tactics were adopted. First, the 3D self-assembly of water-soluble NaCl particles was used as the template for the 3D porous graphene networks and was able to be used as a confining structure to suppress the agglomeration of Sn nanoparticles and promote the growth of graphene walls during the CVD process.
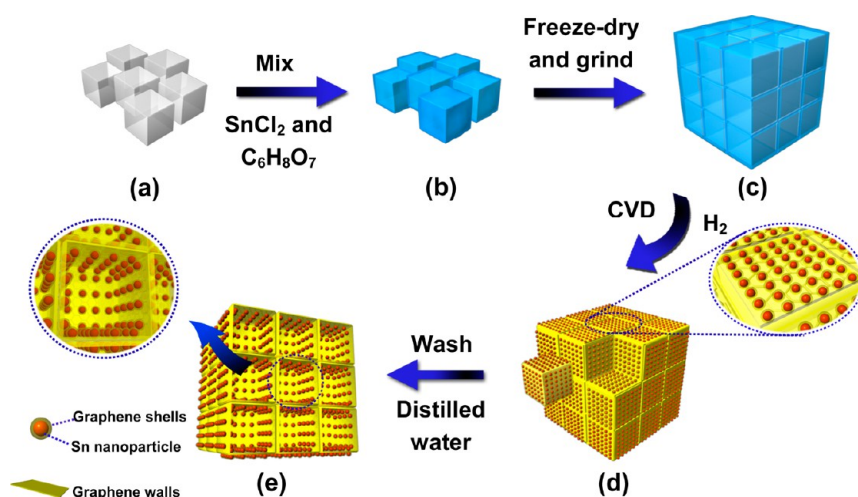
Figure 1. Schematic illustration of the *in situ* CVD process for the one-step synthesis of 3D Sn@G-PGNWs using 3D NaCl self-assembly as a template. (a) NaCl particles. (b) $SnCl_2$–$C_6H_8O_7$-coated NaCl particles. (c) $SnCl_2$–$C_6H_8O_7$-coated NaCl self-assembly. (d) Sn@G-GNW-coated NaCl self-assembly. (e) 3D Sn@G-PGNWs.

It is well known that NaCl has a face-centered cubic (fcc, $Fm3m$ (225), $a = 0.5642$ nm) crystal structure, and its growth rate can be controlled by varying the temperature and concentration.[48,49] Second, environmentally friendly citric acid ($C_6H_8O_7$) was chosen as the carbon precursor because it can restrain the hydrolysis of $SnCl_2$ and also can easily form an even dispersion with the metal precursor ($SnCl_2$) because of the strong interactions between the functional groups of citric acid and the Sn ions in the $SnCl_2$ solution. In the synthesis, the NaCl, citric acid, and $SnCl_2$ were first dissolved in distilled water to get a homogeneous solution,[50] which was subsequently subjected to freeze-drying. During the freeze-drying process, the NaCl particles uniformly coated with an ultrathin $SnCl_2$–$C_6H_8O_7$ complex film, which was induced by the chelation between metal ions and the functional groups of citric acid, were self-assembled into a 3D structure due to their cubic structural characteristic. Upon heating the 3D $SnCl_2$–$C_6H_8O_7$/NaCl at high temperature under H_2 (*i.e.*, CVD process), the Sn ions were reduced to small and uniform Sn nanoparticles due to the confining effect of NaCl surfaces, and then these Sn nanoparticles catalyze the growth of graphene walls and shells using citric acid as a solid carbon source. This procedure is supported by a previous work,[35] in which the graphene nanosheets were synthesized by CVD over the surfaces of Sn nanosheets using glucose as a carbon source. After removing NaCl with distilled water, pure 3D Sn@G-PGNWs with high electrical conductivity and large surface area were easily obtained. In general, Sn–graphene hybrids produced in liquid phase solvents require tedious purification processes, and severe agglomeration of the solid powders finally obtained is very difficult to avoid.[27−31] The solid-phase CVD synthesis approach utilized here is a facile and low-cost way to prepare 3D porous graphene networks anchored with graphene-encapsulated active materials

directly in large scales, which would be very favorable for the wide application of these 3D Sn@G-PGNWs as anode materials for LIBs.[50] Moreover, this one-step *in situ* and high-yield strategy can also be extended to prepare high-quality 3D porous graphene networks by using other metal (Fe, Ni, *etc.*) precursors as a catalyst and build a variety of other interesting 3D porous graphene−metal (or metal oxide) hybrids for potential applications in catalysis, sensor, and energy fields.

An X-ray diffraction (XRD) experiment was first performed to reveal the crystallographic structure of the products (Sn@G-PGNWs). As shown in Figure 2a, all intense and distinct peaks in the pattern can be well ascribed to a β-Sn crystal structure (JCPDS No. 04-0673), and the sharpness of the diffraction peaks implies that the tin phase in the products is well crystallized.[35] The weak and broad peak appearing in the range 17−28° was attributed to the graphene materials in the products. The average Sn particle size calculated from the largest (200) diffraction peak according to the Scherrer equation is about 16.9 nm. To gain insight into the chemical composition, thermogravimetric analysis (TGA) and differential thermal analysis (DTA) were performed on the 3D Sn@G-PGNWs (Figure 2b). The sample is annealed under air to oxidize Sn to SnO_2 (see Supporting Information, Figure S1a) and carbon to CO_2. On the basis of the final weight of SnO_2, the original content of Sn is calculated to be 46.8 wt %.

The morphology of the 3D Sn@G-PGNWs was primarily investigated by scanning electron microscopy (SEM). From SEM images of Figure 2c and d, it can be discerned that the product has unique interconnected submicrometer-sized macroporous networks, and the walls of the interconnected 3D porous networks demonstrate a clear curved profile and a very low contrast, which arise from the ultrathin thickness ($\leq$3 nm) and high mechanical flexibility of the walls composed of a
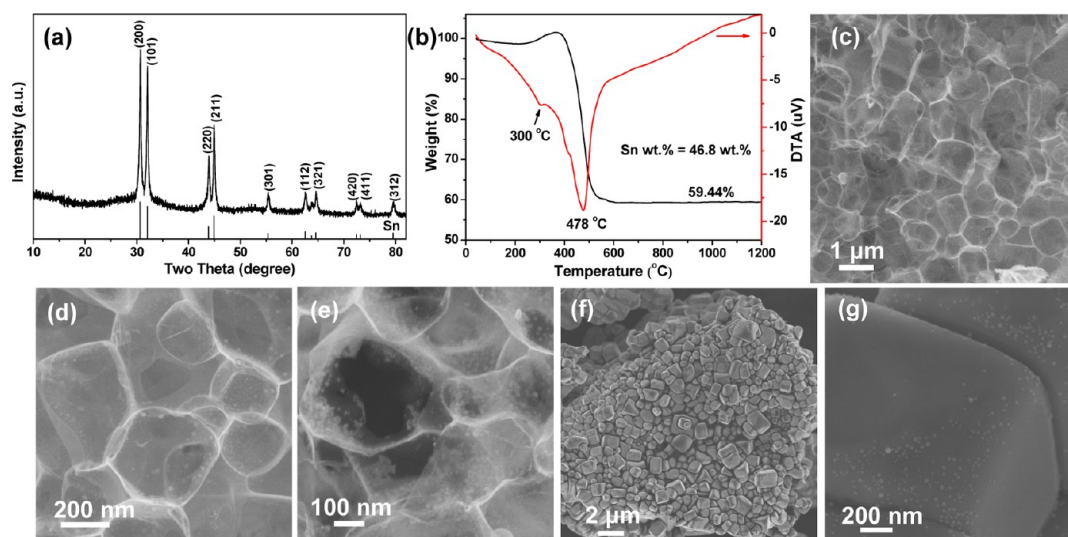
Figure 2. (a) XRD pattern, (b) TGA and DTA profiles, and (c−e) SEM images of 3D Sn@G-PGNWs. (f, g) SEM images of the CVD-synthesized products before eliminating NaCl.

few graphene layers.[39−41] High-magnification SEM image of Figure 2e shows that many uniform Sn@G nanoparticles (5−30 nm) were very homogeneously and closely anchored on the walls of porous graphene networks. It is important to note that no 3D porous graphene networks could be obtained without using NaCl as a template, suggesting that the NaCl plays a crucial role in the synthesis of 3D Sn@G-PGNWs. In order to disclose the influence of NaCl on the formation of this unique 3D architecture, we have investigated in detail the CVD products of the mixture ($SnCl_2$ and $C_6H_8O_7$) without NaCl, the complex of $SnCl_2$−$C_6H_8O_7$/NaCl after the freeze-drying process, and the CVD-synthesized products before eliminating NaCl by SEM and transmission electron microscopy (TEM). As shown in Figure S1b and Figure S2, the as-synthesized products obtained without using NaCl seem to be 3D micrometer-sized amorphous carbon blocks with large Sn particles (>200 nm) embedded (indicated by Sn/C composite), and no 3D graphene networks can be found in the product. This result suggests that during the CVD process without using NaCl the Sn, with a low melting point, is very easily aggregated to large particles, which would have very low catalytic ability to induce the growth of graphene materials and thus only result in the formation of amorphous carbon blocks in the products.[7−10,35−37] When observing the SEM images (see Figure S3a and b) of the complex of $SnCl_2$−$C_6H_8O_7$/NaCl after the freeze-drying process, we found that the NaCl particles uniformly coated with an ultrathin film of $SnCl_2$−$C_6H_8O_7$ were self-assembled into a 3D structure. When investigating the SEM images (see Figure 2f,g and Figure S3c,d) of the CVD-synthesized products before eliminating NaCl, we further observed that the 3D self-assembly was well preserved after the CVD process and the 3D Sn@G-PGNWs were actually formed on the surface of 3D NaCl self-assembly, demonstrating that the 3D NaCl

self-assembly provides a surface for directing the synthesis of the 3D porous graphene networks as well as acts as the confining structure to prevent the aggregation of Sn nanoparticles during the CVD process. Generally, carbonizing the mixture of citric acid and $SnCl_2$ leads to amorphous carbon blocks with Sn particles embedded (see Figure S2) other than porous graphene materials due to the three-dimensional cross-linked structure.[41] Herein, the addition of a mass of NaCl particles could provide a surface for directing the formation of an ultrathin $SnCl_2$−$C_6H_8O_7$ coating and thus alter the three-dimensional cross-linkage state of the citric acid.[41] In the freeze-drying process, these NaCl particles coated with an ultrathin $SnCl_2$−$C_6H_8O_7$ film were self-assembled into a 3D structure, and then during the CVD process, this 3D NaCl self-assembly can act as a confining structure to induce the occurrence of small and uniform Sn nanoparticles with high catalytic activity,[34−36] which catalyze the growth of graphene walls between NaCl surfaces and graphene shells around Sn nanoparticles.[35] As a result, after CVD and eliminating the template of NaCl self-assembly by a simple washing process, pure 3D porous graphene networks anchored with Sn@G nanoparticles can be easily obtained. We also found that the pore sizes and wall thicknesses of the porous graphene or the size and content of the metal can be easily controlled by controlling the content and size of the NaCl and the ratio of metal precursor ($SnCl_2$) to carbon precursor (citric acid). When using NaCl with higher content and larger size as a template, porous graphene networks with thinner walls and larger pores can be synthesized. Meanwhile, when using a higher ratio of $SnCl_2$ to citric acid, larger size and content of Sn nanoparticles within the hybrids can be obtained.

The microstructures of the 3D Sn@G-PGNWs were further studied by TEM and high-resolution TEM (HRTEM). As shown in Figure 3a and b, a continuous 3D
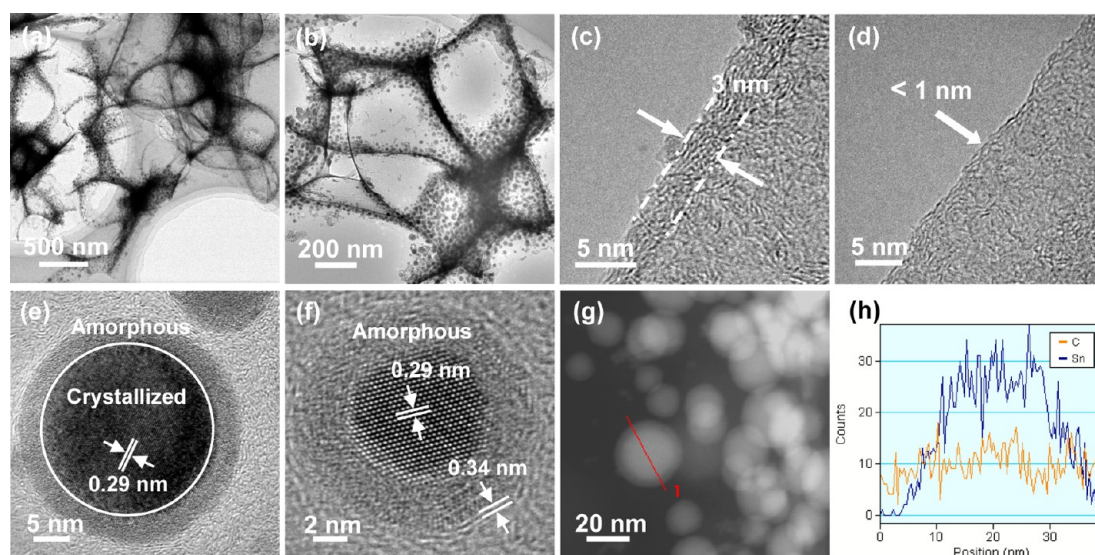
Figure 3. (a, b) TEM images of 3D Sn@G-PGNWs. (c, d) TEM images of walls of porous graphene networks. (e, f) HRTEM images and (g) STEM image of Sn@G nanoparticles. (h) Cross-sectional EDX elemental mapping of point 1 in (g).

ultrathin graphene wall-constructed porous network anchored with uniform Sn@G nanoparticles (5−30 nm) is observed, in good agreement with the SEM observations above. Moreover, when the product was subjected to sonication for a very long time during the TEM sample preparation process, the nanoparticles are still tightly pinned on the graphene walls with a high density (see Figure S4a−d), indicating the strong interaction between Sn@G nanoparticles and graphene walls.[51−54] We hypothesize that such a strong interaction combined with excellent mechanical flexibility of CVD-synthesized graphene walls is very crucial for improving the electrochemical cycling stability due to the fact that these advantages can effectively prevent the agglomeration of Sn@G nanoparticles and thus be very beneficial for maintaining the overall structural integrity. Meanwhile, the strong pinning of Sn@G nanoparticles on the walls of porous graphene networks also facilitates rapid transport of electrons and ions from the graphene walls to the Sn@G nanoparticles for enhancing the electrochemical rate performance.[51−54] Figure 3c and d show HRTEM images of the walls of porous graphene networks. As can be seen, the thickness of the walls consisting of a few graphene layers is about 3 nm or less than 3 nm (Figure 3c and Figure S5a,b); nevertheless, graphene walls with a thickness less than 1 nm also exist (Figure 3d). Figure 3e,f and Figure S5c−f show HRTEM images of Sn@G nanoparticles. It can be observed clearly that these nanoparticles have a core−shell structure, in which the Sn nanoparticle is perfectly encapsulated by graphene shells (∼1 nm) tightly anchored on the graphene walls. Moreover, when investigating the Sn nanoparticles in detail by HRTEM (Figure 3e and Figure S5c−e), we further found that many Sn nanoparticles also have a core−shell structure, in which their central

section is highly crystallized, but their fringe part is amorphous. We speculated that this crystallized-amorphous core−shell structure of Sn nanoparticles might be attributed to the rapid cooling process during CVD. The HRTEM images of Figure 3e,f and Figure S5c−f exhibit clear lattice fringe for a core−shell structure. The spacing of the adjacent lattice planes for the shell is 0.34 nm, corresponding to (002) planes of graphite, while the spacing of the adjacent lattice planes for the core is 0.29 nm, consistent with the (200) plane of Sn crystal. Selected area electronic diffraction (SAED) (Figure S3g), STEM image (Figure 3g), and cross sectional composition line profiles (Figure 3h) further manifest the Sn−graphene core−shell structure.

The characteristic and quality of the graphene in the 3D Sn@G-PGNWs were further evaluated using Raman spectroscopy. The spectrum of Figure 4a obviously reveals the presence of a G band at 1586 cm^{-1}, a 2D band at 2700 cm^{-1}, and a D band at 1350 cm^{-1}. The G band is the result of a radial C−C stretching mode of sp^2-bonded carbon, the 2D band is associated with a second-order zone boundary phonon mode for graphene, and the D band is a first-order zone boundary phonon mode associated with defects in the graphene or graphene edge.[25,26] The shape and intensity of the 2D band are very sensitive to the characteristic and quality of the graphene layers.[25,26] According to Figure 4a, the relative intensities of the G band to the D band (I_G/I_D) and the 2D band to the G band (I_G/I_D) are about 1.18 and 0.62, respectively, which are much higher than that of previous works in graphene,[38,44] indicating a relatively high quality of the few-layer graphene materials in the 3D Sn@G-PGNWs,[43−45] in good agreement with HRTEM investigations above. The pore structure of the 3D architectures is investigated by N$_2$ adsorption−desorption isotherms.
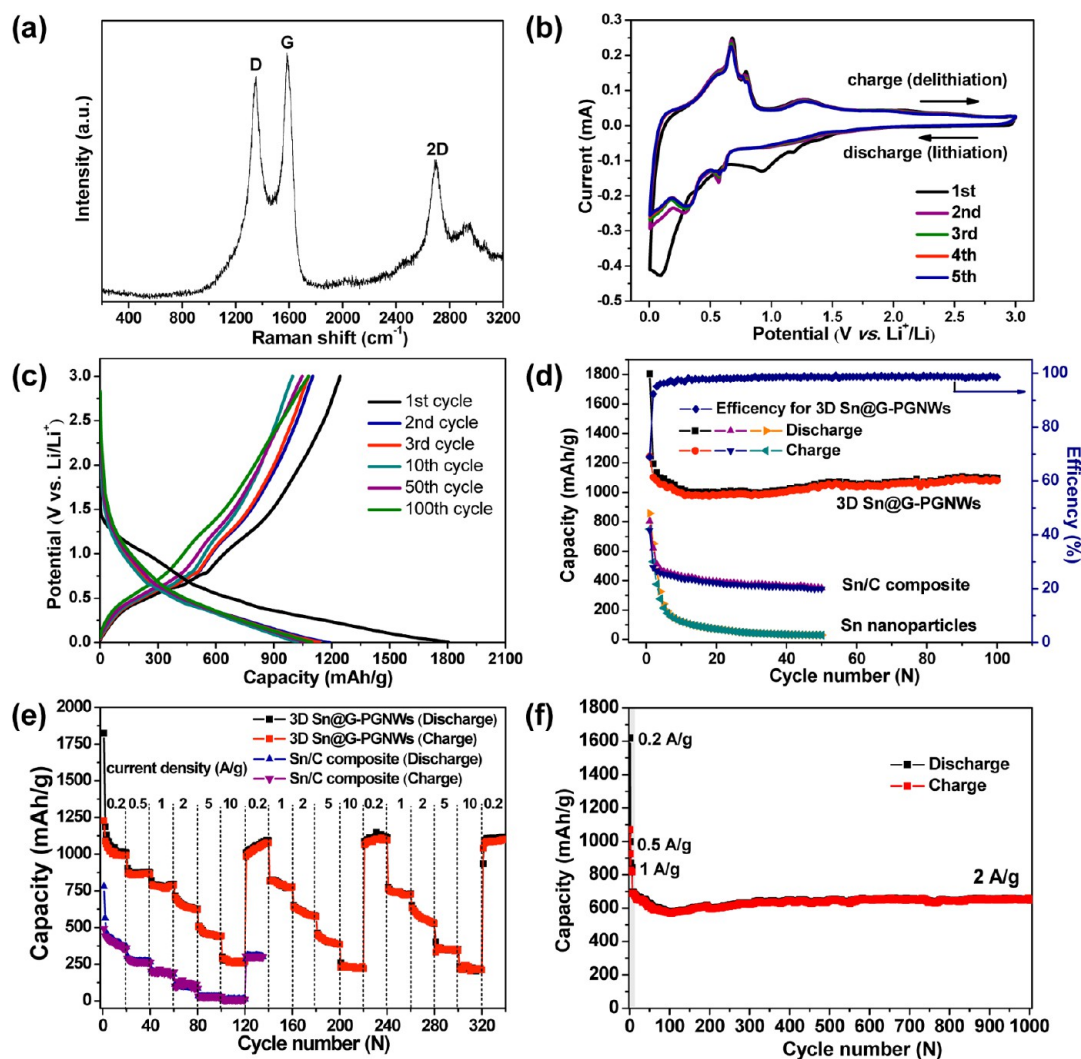
Figure 4. (a) Raman spectrum of 3D Sn@G-PGNWs. (b) CV curves of the 3D Sn@G-PGNW electrode at a voltage range of 0.005 to 3.0 V and scan rate of 0.1 mV/s. (c) Voltage profiles of the 3D Sn@G-PGNW electrode at a current density of 0.2 A/g. (d) Cycle performance of the 3D Sn@G-PGNWs, Sn/C composite, and commercial Sn nanoparticles at a current density of 0.2 A/g. (e) Rate cycle performance of the electrodes of 3D Sn@G-PGNWs and Sn/C composite at charge/discharge rates from 0.2 to 10 C (1 C = 1 A/g) for 340 cycles. (f) Cycle performance of the 3D Sn@G-PGNW electrode at current densities of 0.2, 0.5, and 1 A/g for the initial six cycles and then 2 A/g for the subsequent 1000 cycles.

As shown in Figure S6a, the adsorption−desorption curve exhibits a typical IV isotherm with a hysteresis loop in the P/P_0 range of 0.45−0.98, suggesting the existence of micropores and mesopores in the framework of the 3D hybrid material. The hierarchical pore structure of the 3D Sn@G-PGNWs is further verified by Barrett−Joyner−Halenda (BJH) calculations (see Figure S6b). A broad pore size distribution from 0.5 to 36 nm can be seen, which includes micropores and mesopores, except for the macropores observed in the SEM images of Figure 2c−e. These pores with a size in the range 0.5−36 nm may be attributed to the defects and porous structure in the graphene walls induced by the catalyzation effect of Sn or the rapid gas emission during the CVD process. Brunauer−Emmett−Teller (BET) analysis demonstrates a specific surface area of 365 m^2/g for the 3D Sn@G-PGNWs, which is much larger than that of commercial Sn nanoparticles

(∼6 m^2/g) and Sn/C composite synthesized without using NaCl (∼150 m^2/g).

Coin half-cells using lithium metal as the counter electrode were employed to evaluate the electrochemical performance of the 3D Sn@G-PGNWs. Figure 4b presents representative cyclic voltammograms (CVs) of the initial five cycles at a sweep rate of 0.1 mV/s between 0.005 and 3.0 V. In accord with previous reports,[6,14,16,33,35] it can be seen that the CV curve especially for the discharge branch in the first cycle is very different from that of subsequent cycles.[41,42] Two well-defined waves at 0.92 and 0.085 V are found during the first discharge but disappeared in the subsequent cycles, which is usually attributed to the occurrence of some irreversible reactions associated with formation of an SEI film and the lithium alloying with tin, forming Li_xSn alloys ($Sn + xLi^+ + xe^- \rightarrow Li_xSn$). Furthermore, the absence of irreversible peaks at

1.05 and 1.55 V induced by catalytic decomposition of the electrolyte on metallic Sn implies that Sn was perfectly encapsulated in a graphene shell.[6,14,16,33,35] After the first cycle, the distinct cathodic current peaks at 0.30 and 0.58 V during discharge and the distinct anodic peaks at 0.68, 0.80, and 1.29 V during charge correspond to lithium alloying and dealloying with Sn, respectively, in accord with previous reports on Sn-based anodes.[6,14,16,33,35] Note that after the first cycle the CV curves from the second scan to the fifth scan are well overlapped, suggesting that a stable SEI formed on the graphene shell surfaces during the first cycle can restrain the direct contact of Sn cores with electrolyte and maintain the structural integrity of the Sn@G nanoparticles during the subsequent cycles, thereby resulting in excellent reversibility of the Sn@G-PGNW electrode.[6,14,16,33,35,41,42]

Typical galvanostatic charge/discharge curves of the 3D Sn@G-PGNW electrodes at a current density of 0.2 A/g are shown in Figure 4c. The initial charge and discharge capacities are approximately 1245 and 1805 mAh/g, respectively, resulting in an initial Coulombic efficiency of ∼69%. The initial irreversible capacity loss of the Sn@G-PGNWs could be associated with the inevitable formation of SEI and decomposition of electrolyte,[6,14,16,33,35,41,42] in good agreement with the above CV results (as shown in Figure 4b). It is important to note that both charge and discharge profiles exhibit little change from the second to the 100th cycles, further demonstrating that the 3D Sn@G-PGNW electrodes are very stable during cycling.[6,14,16,33,35,41,42] Figure 4d exhibits cycle performances of Sn@G-PGNWs, commercial Sn nanoparticles, and Sn/C composite produced without using NaCl at a current density of 0.2 A/g. As can be seen, the Sn@G-PGNW electrode shows superior cycling performance, delivering a high reversible capacity of 1089 mAh/g after 100 cycles, which is about 99% of the reversible capacity in the second cycle. Moreover, their Coulombic efficiency is also very excellent, which rapidly increases from 69% in the first cycle to 97% in the fourth cycles and remains above 99% during the subsequent cycles, indicating a facile insertion/extraction of lithium ions as well as efficient transport of electrons and ions in our hybrid anodes.[33,35,41,55] In contrast, a much lower reversible capacity (∼340 mAh/g) of the Sn/C composite is delivered at the end of the 50 cycles. As for the pure Sn nanoparticles, they exhibit very fast capacity fading and have a very low reversible capacity of ∼30 mAh/g after the 50th cycle. Therefore, the 3D Sn@G-PGNW hybrid anode demonstrates remarkably higher reversible capacity and cycling stability, which are ascribed largely to the strong synergistic effect between 3D porous graphene networks and graphene-encapsulated Sn nanostructures. During the charge/discharge process, the graphene shell around Sn nanoparticles is very beneficial for the

growth of a stable SEI film and thus can prevent the rupture of the SEI during cycling, leading to excellent cycling stability. As for the graphene walls with high mechanical flexibility, they can tightly anchor the core–shell structure of Sn@G and thus can restrain the agglomeration of Sn@G nanoparticles to large particles, which is also very helpful for enhancing the cycling stability.[41,42,47,53] In addition, the 3D graphene networks with a porous feature and integrative characteristic can lead to a high contact area between the electrode and electrolyte, which is highly favorable for the efficient access of the electrolyte into the electrode interior and the rapid transport of ions into the deep portions of the Sn@G nanoparticles and the graphene layers. Moreover, this 3D porous framework is also beneficial for the electrochemical adsorption of lithium ions on both sides of ultrathin graphene walls.[50] All these advantages induce high reversible storage capability of the 3D Sn@G-PGNW electrode.

The rate performance of LIB anodes is highly crucial especially for high-power applications in power grids and electric vehicles.[1] The rate and rate cycle performances of the 3D Sn@G-PGNWs up to 10 C rate (1 C = 1 A/g) were studied in the potential window of 0.005 to 3.0 V, as shown in Figure 4e and Table S1. A durable and stable rate capacity at different charge/discharge rates is observed. In the first rate cycle, the average reversible capacities are 1022, 865, 780, 652, 459, and 270 mAh/g for 0.2, 0.5, 1, 2, 5, and 10 C, respectively, and the corresponding energy and power densities for different charge/discharge rates are demonstrated in the Ragone plot of Figure S8a. When the current rate decreased from 10 A/g to 0.2 A/g after the third rate cycle, a capacity of 1040 mAh/g was still recoverable and sustainable up to the 340th cycle without any losses (1076 mAh/g at the 340th cycle), indicating that the Sn@G-PGNW hybrid anode remained very stable during the extended rate cycling process. However, the Sn/C composite anode exhibits a remarkably lower rate capacity (see Figure 4e and Table S1), further confirming the predominance of this unique 3D porous graphene network combined with graphene encapsulation structure for lithium storage. Moreover, the long-term cycling stability at a high rate of 2 C (2 A/g) of the 3D Sn@G-PGNW electrode has also been explored, and the result is shown in Figure 4f. It is striking to note that the specific capacity can reach as high as 682 mAh/g at the rate of 2 A/g and remains approximately 96.3% (657 mAh/g) even after 1000 cycles. The extremely high specific capacity and superior capacity retention achieved at such a high rate (2 A/g) are much larger than previously reported works on Sn nanostructures, Sn/carbon, and Sn–graphene hybrids (as shown in Figure S7 and Table S2).[4−24,27−38] To the best of our knowledge, no Sn-based LIB anodes previously reported can endure hundreds of charge/discharge cycles at high rates. As a matter of fact, most
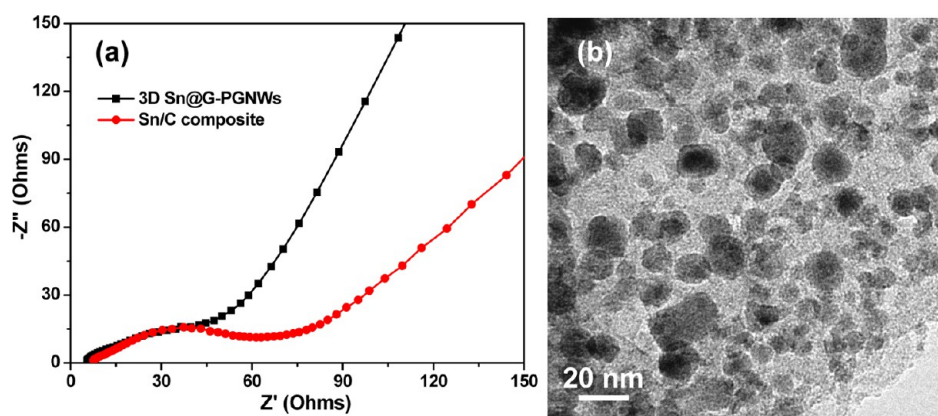
Figure 5. (a) Nyquist plots of 3D Sn@G-PGNWs and Sn/C composite at fresh coin cells over the frequency range from 100 kHz to 0.01 Hz. (b) Typical TEM image of a 3D Sn@G-PGNW hybrid electrode after 340 electrochemical cycles for the rate cycle performance test in Figure 4e.

of these Sn-based LIB anodes exhibit cycle life less than 200 cycles at a current density between 0.05 and 2 A/g, and their capacity retention is also general (see Table S2).[4−24,27−38]

In order to understand the reasons for the much higher rate performance of the 3D Sn@G-PGNWs than that of the Sn/C composite, the impedances of the 3D Sn@G-PGNWs and Sn/C composite at fresh coin cells were investigated using electrochemical impedance spectroscopy (EIS), and the results are displayed in Figure 5a. As can be seen, the two impedance spectra have similar features: a medium-to-high-frequency depressed semicircle and a low-frequency linear tail, which is consistent with impedance spectra of the previous Sn-based anodes.[18,27] The semicircle at high frequency is an indication of SEI resistance (R_{SEI}) and contact resistance (R_f), the semicircle across the medium-frequency region represents the charge-transfer impedance (R_{ct}) on the electrode/electrolyte interface, and the low-frequency linear tail corresponds to the Warburg impedance (Z_w) associated with the diffusion of lithium ions in the bulk electrode (R_e).[40,41,47,55] According to Figure 5a, it can be found clearly that the diameter of the semicircle for the 3D Sn@G-PGNW electrode in the high-medium-frequency region is significantly smaller than that of the Sn/C composite, which illustrates the superior rate performance of the 3D Sn@G-PGNW hybrid anode as well as implies that the CVD-synthesized graphene and 3D porous graphene structure could effectively enhance the electrical conductivity and reduce the contact and charge-transfer resistances in the Sn@G-PGNW electrode.[40,41,47,55]

The morphology and structure change of the 3D Sn@G-PGNW electrode after deep charge/discharge cycles were explored by TEM. Figure 5b and Figure S8b show TEM images of the 3D Sn@G-PGNW hybrid anode after rate cycling for 340 cycles (as shown in Figure 4e). Although the sample surface is covered with a thick and gel-like SEI layer, it can be seen clearly that the individual nanoparticles with diameter in the

range 5−30 nm have not aggregated at all and still anchor homogeneously and firmly to the surface of the graphene walls, which is very similar to the morphology of the pristine product (see Figure 3b and Figure S4). This evidence implies that the strong interaction between Sn@G nanoparticles and graphene walls as well as the superior mechanical flexibility of CVD-synthesized graphene walls can restrain the substantial aggregation of Sn@G nanoparticles and the cracking of the electrode material during deep charge/discharge cycling, leading to extremely excellent cycling stability.[23,53] In addition, the thin graphene shell with high elasticity can effectively buffer the mechanical stress resulting from the severe volume change of Sn nanoparticles during lithium ion insertion/extraction, which is also very beneficial for improving the cycling performance of the 3D Sn@G-PGNW electrode.[41,42]

The above results clearly confirm that our 3D Sn@G-PGNWs hybrid anode has superior cycle and rate performance, which can be ascribed to the following factors. First, the small Sn nanoparticles can offer a great deal of active sites for lithium ion storage and a short pathway for lithium ion transport, resulting in high reversible capacity and rate performance. Second, the CVD-synthesized graphene shells with high mechanical flexibility can not only prevent the Sn cores from directly contacting the electrolyte and alleviate the side reactions at the interface between Sn and electrolyte but also suppress the aggregation of Sn nanoparticles and accommodate the volume expansion, leading to structural and interfacial stabilization of Sn nanoparticles.[41,42] Third, the highly robust and elastic graphene networks synthesized by *in situ* CVD function as a buffer that reinforce the structural integrity of the overall electrode *via* tightly pinning the Sn@G core−shell nanostructures, thereby leading to excellent cycling stability. Fourth, the overall graphene networks with superior electrical conductivity, 3D porous nature, and large surface area can significantly

facilitate the diffusion and transport of electrons and ions, contributing to the remarkable improvements on the reversible capacity and rate capability. On the basis of the analyses presented above, we believe that the outstanding synergetic effect between the porous graphene networks and the Sn@G core–shell nanostructures induces the superior lithium storage performance of the overall electrode by maximally utilizing the electrochemically active graphene and Sn nanoparticles.[47,53,54]

CONCLUSIONS

In summary, novel 3D porous graphene networks anchored with small and uniform Sn nanoparticles (5–30 nm) encapsulated with graphene shells (~1 nm) were fabricated by a facile and scalable one-step *in situ* CVD method using metal precursors as a catalyst and a three-dimensional self-assembly of NaCl particles as a template. In this unique 3D architecture, the CVD-synthesized graphene shells with high elasticity can effectively preserve the structural and interfacial stabilization of Sn nanoparticles as well as accommodate the mechanical stress resulting from the severe volume change of Sn nanoparticles during lithium ion insertion/extraction, while the interconnected 3D porous graphene networks with superior electrical conductivity, high mechanical flexibility, and large surface area tightly pin the Sn@G core–shell structure, thereby leading to remarkably enhanced structural and electrical integrity as well as excellent kinetics for ion and electron transport of the overall electrode. As a result, long-term cyclic stability at high rates (a high capacity of 682 mAh/g is achieved at 2 A/g and is maintained at approximately 96.3% even after 1000 cycles) and superior rate capability (1022 mAh/g at 0.2 C, 865 mAh/g at 0.5 C, 780 mAh/g at 1 C, 652 mAh/g at 2 C, 459 mAh/g at 5 C, and 270 mAh/g at 10 C, 1 C = 1 A/g) were achieved when 3D Sn@G-PGNWs were used as an LIB anode, which is the best one ever reported for Sn-based LIB anodes to date. Moreover, this one-step *in situ* CVD protocol can also be extended to preparing high-quality 3D porous graphene networks by using other metal (Fe, Ni, *etc*.) precursors as a catalyst and building other 3D porous graphene–metal (or metal oxide) hybrids for potential applications in catalysis, sensors, and energy fields.

METHODS

Synthesis of 3D Sn@G-PGNWs. The reagents were purchased from Tianjin Chemical Reagent Company and used without further purification. For preparing 3D Sn@G-PGNWs, 2.5 g of citric acid, 0.384 g of $SnCl_2 \cdot 2H_2O$, and 14.7 g of NaCl were dissolved in 50 mL of deionized water by magnetic stirring. The obtained solution was frozen in a refrigerator at −20 °C for 24 h. The water in the resulting gel is eliminated by a freeze-drying technology, and then the dry gel was ground to a fine composite powder (≥100 mesh). For the CVD synthesis, 10 g of the composite powder in a quartz boat was annealed at 750 °C for 2 h under H_2 and then cooled rapidly (within 2 min) to room temperature under the protection of H_2. The as-synthesized products were washed with deionized water several times to remove NaCl, and then pure 3D Sn@G-PGNWs were obtained. For comparison, amorphous carbon blocks with Sn particles embedded (Sn/C composite) were also synthesized by carbonizing the mixture of $SnCl_2$ and citric acid without NaCl at the same conditions as those for fabricating 3D Sn@G-PGNWs.[41,50]

Characterization Techniques. XRD measurements were taken on a Rigaku D/max diffractometer with Cu Kα radiation at a wavelength of 1.5406 Å to determine the phase composition and crystallinity. SEM and TEM were performed on a JSM-6700F and FEI Tecnai G² F20, respectively, to investigate the morphology and microstructure. TGA and DTA were performed with a Perkin-Elmer (TA Instruments) instrument up to 1200 °C at a heating rate of 10 °C/min in air. The Raman spectrum was recorded on the LabRAM HR Raman spectrometer using laser excitation at 514.5 nm from an argon ion laser source to validate the graphene materials in the 3D Sn@G-PGNWs. Nitrogen sorption isotherms and BET surface area were measured at 77 K with an ASAP 2020 physisorption analyzer (USA).

Electrochemical Measurement. Electrochemical measurements were conducted using a coin-type test cell (CR2032) with lithium metal working as both counter and reference electrode. The working electrode was composed of active materials (3D Sn@G-PGNWs, Sn/C composite, or Sn nanoparticles of ~60 nm purchased from DK Nanotechnology Co. LTD, Beijing), conductivity agent (carbon black), and binder (polyvinylidene fluoride) in a weight ratio of 80:10:10 on a copper foil. The electrolyte was $LiPF_6$ (1 M) in ethylene carbonate/dimethyl carbonate/diethyl carbonate (1:1:1 vol%). The cell assembly was conducted in an Ar-filled glovebox. CV measurement was conducted at 0.1 mV/s within 0.005–3.0 V on a CHI660D electrochemical workstation. Galvanostatic charge/discharge cycles were tested by a LAND CT2001A electrochemical workstation at various current densities of 200 mA/g (0.2 C) to 10 A/g (10 C) between 3.00 and 0.005 V. All of the specific capacities here were calculated on the basis of the total weight of the 3D Sn@G-PGNWs, Sn/C composite, or Sn nanoparticles. Electrochemical impedance spectroscopy measurements were performed using a CHI660D electrochemical workstation by employing an ac voltage of 5 mV amplitude in the frequency range 0.1–100 kHz.[41,50]

Supporting Information Available: Supplementary SEM and TEM images, EDS, SAED, and BET analyses. This material is available free of charge *via* the Internet at http://pubs.acs.org.

REFERENCES AND NOTES

1. Armand, M.; Tarascon, J. M. Building Better Batteries. *Nature* **2008**, *451*, 652–657.
2. Wang, B.; Luo, B.; Li, X. L.; Zhi, L. J. The Dimensionality of Sn Anodes in Li-Ion Batteries. *Mater. Today* **2012**, *15*, 544–552.
3. Hua, R. Z.; Zhu, M.; Wang, H.; Liu, J. W.; Liuzhang, O.; Zou, J. Sn Buffered by Shape Memory Effect of NiTi Alloys as High-Performance Anodes for Lithium Ion Batteries. *Acta Mater.* **2012**, *60*, 4695–4703.

4. Kravchyk, K. V.; Protesescu, L.; Bodnarchuk, M. I.; Krumeich, F.; Yarema, M.; Walter, M.; Guntlin, Ch.; Kovalenko, M. V. Monodisperse and Inorganically Capped Sn and Sn/SnO₂ Nanocrystals for High Performance Li-Ion Battery Anodes. *J. Am. Chem. Soc.* **2013**, *135*, 4199–4202.

5. Xu, L. P.; Kim, C.; Shukla, A. K.; Dong, A.; Mattox, T. M.; Milliron, D. J.; Cabana, J. Monodisperse Sn Nanocrystals as a Platform for the Study of Mechanical Damage during Electrochemical Reactions with Li. *Nano Lett.* **2013**, *13*, 1800–1805.

6. Xu, Y. H.; Liu, Q.; Zhu, Y. J.; Liu, Y. H.; Langrock, A.; Zachariah, M. R.; Wang, C. S. Uniform Nano-Sn/C Composite Anodes for Lithium Ion Batteries. *Nano Lett.* **2013**, *13*, 470–474.

7. Xu, Y. H.; Guo, J. C.; Wang, C. S. Sponge-Like Porous Carbon/Tin Composite Anode Materials for Lithium Ion Batteries. *J. Mater. Chem.* **2012**, *22*, 9562–9567.

8. Yu, Y.; Gu, L.; Zhu, C.; Van Aken, P. A.; Maier, J. Tin Nanoparticles Encapsulated in Porous Multichannel Carbon Microtubes: Preparation by Single-Nozzle Electrospinning and Application as Anode Material for High-Performance Li-Based Batteries. *J. Am. Chem. Soc.* **2009**, *131*, 15984–15985.

9. Derrien, G.; Hassoun, J.; Panero, S.; Scrosati, B. Nanostructured Sn-C Composite as an Advanced Anode Material in High-Performance Lithium-Ion Batteries. *Adv. Mater.* **2007**, *19*, 2336–2340.

10. Hassoun, J.; Lee, K. S.; Sun, Y. K.; Scrosati, B. An Advanced Lithium Ion Battery Based on High Performance Electrode Materials. *J. Am. Chem. Soc.* **2011**, *133*, 3139–3143.

11. Hassoun, J.; Derrien, G.; Panero, S.; Scrosati, B. A Nanostructured Sn-C Composite Lithium Battery Electrode with Unique Stability and High Electrochemical Performance. *Adv. Mater.* **2008**, *20*, 3169–3175.

12. Qiu, Y. C.; Yan, K. Y.; Yang, S. H. Ultrafine Tin Nanocrystallites Encapsulated in Mesoporous Carbon Nanowires: Scalable Synthesis and Excellent Electrochemical Properties for Rechargeable Lithium Ion Batteries. *Chem. Commun.* **2010**, *46*, 8359–8361.

13. Wang, Y. G.; Li, B.; Zhang, C. L.; Tao, H.; Kang, S. F.; Jiang, S.; Li, X. Simple Synthesis of Metallic Sn Nanocrystals Embedded in Graphitic Ordered Mesoporous Carbon Walls as Superior Anode Materials for Lithium Ion Batteries. *J. Power Sources* **2012**, *219*, 89–93.

14. Hwang, J. K.; Woo, S. H.; Shim, J. M.; Jo, C. S.; Lee, K. T.; Lee, J. One-Pot Synthesis of Tin-Embedded Carbon/Silica Nanocomposites for Anode Materials in Lithium-Ion Batteries. *ACS Nano* **2013**, *7*, 1036–1044.

15. Deng, D.; Lee, J. Y. Reversible Storage of Lithium in a Rambutan-Like Tin-Carbon Electrode. *Angew. Chem., Int. Ed.* **2009**, *48*, 1660–1663.

16. Yu, Y.; Gu, L.; Wang, C.; Dhanabalan, A.; van Aken, P. A.; Maier, J. Encapsulation of Sn@Carbon Nanoparticles in Bamboo-Like Hollow Carbon Nanofibers as an Anode Material in Lithium Based Batteries. *Angew. Chem., Int. Ed.* **2009**, *48*, 6485–6489.

17. Wang, Y.; Wu, M. H.; Jiao, Z.; Lee, J. Y. Sn@CNT and Sn@C@CNT Nanostructures for Superior Reversible Lithium Ion Storage. *Chem. Mater.* **2009**, *21*, 3210–3215.

18. Zhang, H. K.; Song, H. H.; Chen, X. H.; Zhou, J. S. Enhanced Lithium Ion Storage Property of Sn Nanoparticles: The Confinement Effect of Few-Walled Carbon Nanotubes. *J. Phys. Chem. C* **2012**, *116*, 22774–22779.

19. Hou, X. Y.; Jiang, H.; Hu, Y. J.; Li, Y. F.; Huo, J. C.; Li, C. Z. *In Situ* Deposition of Hierarchical Architecture Assembly from Sn-Filled CNTs for Lithium-Ion Batteries. *ACS Appl. Mater. Interfaces* **2013**, *5*, 6672–6677.

20. Seo, S. D.; Lee, G. H.; Lim, A. H.; Min, K. M.; Kim, J. C.; Shim, H. W.; Park, K. S.; Kim, D. W. Direct Assembly of Tin−MWCNT 3D-Networked Anode for Rechargeable Lithium Ion Batteries. *RSC Adv.* **2012**, *2*, 3315–3320.

21. Lee, K. T.; Jung, Y. S.; Oh, S. M. Synthesis of Tin-Encapsulated Spherical Hollow Carbon for Anode Material in Lithium Secondary Batteries. *J. Am. Chem. Soc.* **2003**, *125*, 5652–5653.

22. Zhang, W. M.; Hu, J. S.; Guo, Y. G.; Zheng, S. F.; Zhong, L. S.; Song, W. G.; Wan, L. J. Tin-Nanoparticles Encapsulated in Elastic Hollow Carbon Spheres for High-Performance Anode Material in Lithium-Ion Batteries. *Adv. Mater.* **2008**, *20*, 1160–1165.

23. Li, X. F.; Dhanabalan, A.; Gu, L.; Wang, C. L. Three-Dimensional Porous Core-Shell Sn@Carbon Composite Anodes for High-Performance Lithium-Ion Battery Applications. *Adv. Energy Mater.* **2012**, *2*, 238–244.

24. Hsu, K. C.; Liu, C. E.; Chen, P. C.; Lee, C. Y.; Chiu, H. T. One-Step Vapor−Solid Reaction Growth of Sn@C Core−Shell Nanowires as an Anode Material for Li-Ion Batteries. *J. Mater. Chem.* **2012**, *22*, 21533–21539.

25. Lee, G. H.; Cooper, R. C.; An, S. J.; Lee, S.; Zande, A.; Petrone, N.; Hammerberg, A. G.; Lee, C. G.; Crawford, B.; Oliver, W.; *et al*. High-Strength Chemical-Vapor-Deposited Graphene and Grain Boundaries. *Science* **2013**, *340*, 1073–1076.

26. Xue, Y. Z.; Wu, B.; Jiang, L.; Guo, Y. L.; Huang, L. P.; Chen, J. Y.; Tan, J. H.; Geng, D. C.; Luo, B. R.; Hu, W. P.; *et al*. Low Temperature Growth of Highly Nitrogen-Doped Single Crystal Graphene Arrays by Chemical Vapor Deposition. *J. Am. Chem. Soc.* **2012**, *134*, 11060–11063.

27. Wen, Z. H.; Cui, S. M.; Kim, H. J.; Mao, S.; Yu, K. H.; Lu, G. H.; Pu, H. H.; Mao, O.; Chen, J. H. Binding Sn-Based Nanoparticles on Graphene as the Anode of Rechargeable Lithium-Ion Batteries. *J. Mater. Chem.* **2012**, *22*, 3300–3306.

28. Yue, W. B.; Yang, S.; Ren, Y.; Yang, X. J. *In Situ* Growth of Sn, SnO on Graphene Nanosheets and Their Application as Anode Materials for Lithium-Ion Batteries. *Electrochim. Acta* **2013**, *92*, 412–420.

29. Sathish, M.; Mitani, S.; Tomai, T. Nanocrystalline Tin Compounds/Graphene Nanocomposite Electrodes as Anode for Lithium-Ion Battery. *J. Solid State Chem.* **2012**, *16*, 1767–1774.

30. Nithya, C.; Gopukumar, S. Reduced Graphite Oxide/Nano Sn: A Superior Composite Anode Material for Rechargeable Lithium-Ion Batteries. *ChemSusChem* **2013**, *6*, 898–904.

31. Chen, S. Q.; Wang, Y.; Ahn, H. Microwave Hydrothermal Synthesis of High Performance Tin-Graphene Nanocomposites for Lithium Ion Batteries. *J. Power Sources* **2012**, *216*, 22–27.

32. Liang, S. Z.; Zhu, X. F.; Lian, P. C. Superior Cycle Performance of Sn@C/Graphene Nanocomposite as an Anode Material for Lithium-Ion Batteries. *J. Solid State Chem.* **2011**, *184*, 1400–1404.

33. Wang, D. N.; Li, X. F.; Yang, J. L.; Wang, J. J.; Geng, D. S.; Li, R. Y.; Cai, M.; Sham, T. K.; Sun, X. L. Hierarchical Nanostructured Core−Shell Sn@C Nanoparticles Embedded in Graphene Nanosheets: Spectroscopic View and Their Application in Lithium Ion Batteries. *Phys. Chem. Chem. Phys.* **2013**, *15*, 3535–3542.

34. Zou, Y.; Wang, Y. Sn@CNT Nanostructures Rooted in Graphene with High and Fast Li-Storage Capacities. *ACS Nano* **2011**, *5*, 8108–8114.

35. Luo, B.; Wang, B.; Li, X. L.; Jia, Y. Y.; Liang, M. H.; Zhi, L. J. Graphene-Confined Sn Nanosheets with Enhanced Lithium Storage Capability. *Adv. Mater.* **2012**, *24*, 3538–3543.

36. Luo, B.; Wang, B.; Liang, M. H.; Ning, J.; Li, X. L.; Zhi, L. J. Reduced Graphene Oxide-Mediated Growth of Uniform Tin-Core/Carbon-Sheath Coaxial Nanocables with Enhanced Lithium Ion Storage Properties. *Adv. Mater.* **2012**, *24*, 1405–1409.

37. Ji, L. W.; Tan, Z. K.; Kuykendall, T.; An, E. J.; Fu, Y. B.; Battaglia, V.; Zhang, Y. G. Multilayer Nanoassembly of Sn-Nanopillar Arrays Sandwiched between Graphene Layers for High-Capacity Lithium Storage. *Energy Environ. Sci.* **2011**, *4*, 3611–3616.

38. Wang, G. X.; Wang, B.; Wang, X. H.; Park, J.; Dou, S. X.; Ahn, H.; Kim, K. Sn/Graphene Nanocomposite with 3D Architecture for Enhanced Reversible Lithium Storage in Lithium Ion Batteries. *J. Mater. Chem.* **2009**, *19*, 8378–8384.

39. Li, Y. Y.; Li, Z. S.; Shen, P. K. Simultaneous Formation of Ultrahigh Surface Area and Three-Dimensional Hierarchical Porous Graphene-Like Networks for Fast and Highly Stable Supercapacitors. *Adv. Mater.* **2013**, *25*, 2474–2480.

40. Su, Y. Z.; Li, S.; Wu, D. Q.; Zhang, F.; Liang, H. W.; Gao, P. F.; Cheng, C.; Feng, X. L. Two-Dimensional Carbon-Coated Graphene/Metal Oxide Hybrids for Enhanced Lithium Storage. *ACS Nano* **2012**, *6*, 8349–8356.

41. He, C.; Wu, S.; Zhao, N.; Shi, C.; Liu, E.; Li, J. Carbon-Encapsulated Fe_3O_4 Nanoparticles as a High-Rate Lithium Ion Battery Anode Material. *ACS Nano* **2013**, *7*, 4459–4469.

42. Wang, B.; Li, X. L.; Zhang, X. F.; Luo, B.; Jin, M. H.; Liang, M. H.; Dayeh, S. A.; Picraux, S. T.; Zhi, L. J. Adaptable Silicon Carbon Nanocables Sandwiched between Reduced Graphene Oxide Sheets as Lithium Ion Battery Anodes. *ACS Nano* **2013**, *7*, 1437–1445.

43. Chen, Z. P.; Ren, W. C.; Gao, L. B.; Liu, B. L.; Pei, S. F.; Cheng, H. M. Three-Dimensional Flexible and Conductive Interconnected Graphene Networks Grown by Chemical Vapour Deposition. *Nat. Mater.* **2011**, *10*, 424–428.

44. Wang, H.; Sun, K.; Tao, F.; Stacchiola, D. J.; Hu, Y. H. 3D Honeycomb-Like Structured Graphene and Its High Efficiency as a Counter-Electrode Catalyst for Dye-Sensitized Solar Cells. *Angew. Chem., Int. Ed.* **2013**, *52*, 9210–9214.

45. He, Y. M.; Chen, W. J.; Li, X. D.; Zhang, Z. X.; Fu, J. C.; Zhao, C. H.; Xie, E. Q. Freestanding Three-Dimensional Graphene/MnO_2 Composite Networks as Ultralight and Flexible Supercapacitor Electrodes. *ACS Nano* **2013**, *7*, 174–182.

46. Chen, W. F.; Li, S. R.; Chen, C. H.; Yan, L. F. Self-Assembly and Embedding of Nanoparticles by *in Situ* Reduced Graphene for Preparation of a 3D Graphene/Nanoparticle Aerogel. *Adv. Mater.* **2011**, *23*, 5679–5683.

47. Wei, W.; Yang, S. B.; Zhou, H. X.; Lieberwirth, I.; Feng, X. L.; Müllen, K. 3D Graphene Foams Cross-Linked with Pre-Encapsulated Fe_3O_4 Nanospheres for Enhanced Lithium Storage. *Adv. Mater.* **2013**, *25*, 2909–2914.

48. Chakraborty, D.; Patey, G. N. Evidence that Crystal Nucleation in Aqueous NaCl Solution Occurs by the Two-Step Mechanism. *Chem. Phy. Lett.* **2013**, *587*, 25–29.

49. Chakraborty, D.; Patey, G. N. How Crystals Nucleate and Grow in Aqueous NaCl Solution. *J. Phys. Chem. Lett.* **2013**, *4*, 573–578.

50. Chen, L.; Wang, Z. Y.; He, C.; Zhao, N.; Shi, C.; Liu, E.; Li, J. Porous Graphitic Carbon Nanosheets as a High-Rate Anode Material for Lithium Ion Batteries. *ACS Appl. Mater. Interfaces* **2013**, *5*, 9537–9545.

51. Lin, J.; Peng, Z. W.; Xiang, C. S.; Ruan, G. D.; Yan, Z.; Natelson, D.; Tour, J. M. Graphene Nanoribbon and Nanostructured SnO_2 Composite Anodes for Lithium Ion Batteries. *ACS Nano* **2013**, *7*, 6001–6006.

52. Zhou, G. M.; Wang, D. W.; Yin, L. C.; Li, N.; Li, F.; Cheng, H. M. Oxygen Bridges between NiO Nanosheets and Graphene for Improvement of Lithium Storage. *ACS Nano* **2012**, *6*, 3214–3223.

53. Wu, Z. S.; Ren, W. C.; Wen, L.; Gao, L. B.; Zhao, J. P.; Chen, Z. P.; Zhou, G. M.; Li, F.; Cheng, H. M. Graphene Anchored with Co_3O_4 Nanoparticles as Anode of Lithium Ion Batteries with Enhanced Reversible Capacity and Cyclic Performance. *ACS Nano* **2010**, *4*, 3187–3194.

54. Peng, C. X.; Chen, B. D.; Qin, Y.; Yang, S. H.; Li, C. Z.; Zuo, Y. H.; Liu, S. Y.; Yang, J. H. Facile Ultrasonic Synthesis of CoO Quantum Dot/Graphene Nanosheet Composites with High Lithium Storage Capacity. *ACS Nano* **2012**, *6*, 1074–1081.

55. Jia, X. L.; Chen, Z.; Cui, X.; Peng, Y. T.; Wang, X. L.; Wang, G.; Wei, F.; Lu, Y. F. Building Robust Architectures of Carbon and Metal Oxide Nanocrystals toward High-Performance Anodes for Lithium-Ion Batteries. *ACS Nano* **2012**, *6*, 9911–9919.